

Observation of Cosserat elastic effects in a tetragonal negative Poisson's ratio lattice

Z. Rueger, D. Li ^a and R. S. Lakes*

November 10, 2017

Department of Engineering Physics, Department of Materials Science
University of Wisconsin, Madison, WI 53706-1687, USA

Keywords (auxetic, Cosserat, micropolar, generalized continuum)

* Corresponding author. email lakes@engr.wisc.edu Phone: +00 608 265 8697

^a College of Sciences, Northeastern University, Shenyang 110819, PR China

Preprint, Rueger, Z., Li, D., Lakes, R. S., "Observation of Cosserat elastic effects in a tetragonal negative Poisson's ratio lattice" *Physica Status Solidi B*, 1600840, 6 pages, Oct. (2017).

Abstract

Size effects are explored experimentally in a tetragonal lattice structure. Size dependence of rigidity is nonclassical elastic and is interpreted via Cosserat elasticity. The characteristic lengths are about a third the cell size. The Cosserat characteristic length for torsion is $\ell_t = 5.6$ mm. The characteristic length for bending is $\ell_b = 5.4$ mm. The size effect in torsion was a factor 4.5 in rigidity. The ratio of characteristic length to cell size is larger than in fully stretch dominated lattices but smaller than in bend dominated honeycombs or foams.

1 Introduction

The first negative Poisson's ratio materials, honeycombs in 2D [1] and foams in 3D [2] had a structure size sufficiently large to be apparent to the unaided eye. It had been proposed that a coarse structure was required for negative Poisson's ratio [3]. The size of the structure is not, however, pertinent in that context. Poisson's ratio is a concept in classical elasticity which has no length scale [4]. Indeed, in some negative Poisson's ratio materials, particularly those experimentally associated with phase transformations in gels [5] and in polycrystalline quartz [6], the governing structure is on the atomic scale. Analyses of a 2D array of hard hexamer discs indicated the existence of a phase transition between a tilted and a straight phase [7]; results suggested negative Poisson's ratio associated with the transformation to tilted phase. Numerical results also reveal a decrease in Poisson's ratio during phase transformations; such a change is a good indicator of transformation [8] [9]. Structure size is however associated with phenomena such as size dependence of rigidity in torsion and bending (size effects), non-classical values of stress concentration, and dispersion of waves. Continuum theories are widely used to represent physical structured materials to facilitate practical calculations. Classical elasticity is one such theory but not the only one. One may incorporate less freedom as in the uniconstant elasticity theory of Navier [10]. This theory only allowed one elastic constant, a modulus. The analysis assumed that forces act along the lines joining pairs of atoms and that forces are proportional to changes in distance between atoms. The theory predicts a Poisson's ratio of 1/4 for all isotropic materials. Because experiments disclosed

a range of Poisson's ratios, the uniconstant theory was abandoned. Classical isotropic elasticity has two independent elastic constants and allows Poisson's ratio in the range -1 to 1/2. Cosserat elasticity incorporates more freedom than classical elasticity. Cosserat elasticity [11], (with inertia terms called micropolar [12]) allows points to rotate as well as translate. Cosserat elasticity also incorporates a couple stress (a torque per unit area) as well as the force per unit area of classical elasticity. There are six independent elastic constants for the isotropic Cosserat solid and even more if it is anisotropic.

The Cosserat couple stress arises from a superposition of bending and twisting moments that are transmitted by the material's structural elements. The Cosserat micro rotation is associated with the rotation of the structural elements. Bending moments on ribs of honeycomb or foam were analyzed in the classical elastic treatments of foam [13] but no effects of rotation gradients were considered.

The constitutive equations for an anisotropic [12] Cosserat elastic solid are as follows.

$$\sigma_{ij} = C_{ijkl}\epsilon_{kl} + P_{ijkl}\phi_{k,l}, \quad (1)$$

$$m_{ij} = Q_{ijkl}\phi_{k,l} + P_{ijkl}\epsilon_{kl}, \quad (2)$$

Here ϵ_{kl} is strain, σ_{ij} is stress (symmetric in classical elasticity but asymmetric here), C_{ijkl} is the elastic modulus tensor. The usual Einstein summation convention is assumed in which repeated indices are summed over. m_{ij} is the couple stress tensor, moment per unit area, asymmetric in general. P_{ijkl} and Q_{ijkl} are Cosserat elastic constants that provide sensitivity to local gradient of (micro) rotation vector. The Cosserat microrotation vector ϕ_i is kinematically distinct from the macrorotation vector $r_i = (e_{ijk}u_{k,j})/2$ associated with the motion of neighboring points.

The lattice structure under consideration is anisotropic, however isotropic analysis is more developed and provides physical insight. The constitutive equations for an isotropic micropolar solid [12] are:

$$\sigma_{ij} = 2G\epsilon_{ij} + \lambda\epsilon_{kk}\delta_{ij} + \kappa e_{ijk}(r_k - \phi_k) \quad (3)$$

$$m_{ij} = \alpha\phi_{k,k}\delta_{ij} + \beta\phi_{i,j} + \gamma\phi_{j,i} \quad (4)$$

There are six independent elastic constants for an isotropic Cosserat solid. They are λ , G , α , β , γ , κ . It is appropriate to define technical constants as follows. They are helpful for physical insight as is the case comparing tensorial constants and technical constants in classical elasticity.

$$\text{Young's modulus} \quad E = \frac{G(3\lambda + 2G)}{\lambda + G} \quad (5)$$

$$\text{Shear modulus} \quad G \quad (6)$$

$$\text{Poisson's ratio} \quad \nu = \frac{\lambda}{2(\lambda + G)} \quad (7)$$

$$\text{Characteristic length, torsion} \quad \ell_t = \sqrt{\frac{\beta + \gamma}{2G}} \quad (8)$$

$$\text{Characteristic length, bending} \quad \ell_b = \sqrt{\frac{\gamma}{4G}} \quad (9)$$

$$\text{Coupling number} \quad N = \sqrt{\frac{\kappa}{2G + \kappa}} \quad (10)$$

$$\text{Polar ratio} \quad \Psi = \frac{\beta + \gamma}{\alpha + \beta + \gamma}. \quad (11)$$

Stress and strain fields in Cosserat solids differ from classical predictions. For example, size effects occur in the analysis of torsion [14] and bending [15] of circular cylinders of Cosserat elastic cylinders. Slender specimens are stiffer than predicted classically. Small holes in a plate exhibit a lower stress concentration than larger ones [16] in contrast to classical elasticity.

A variety of experiments have disclosed Cosserat elastic effects. Size effects consistent with Cosserat elasticity occur in the torsion and bending of closed cell foams [17, 18], open cell foam [19], negative Poisson's ratio foam [20], and compact bone [21]. These effects are consistent with Cosserat elasticity. Apparent modulus increases as specimen size is reduced. In comparison, classical elasticity predicts apparent modulus independent of specimen thickness. For Cosserat effects to be observable, the material micro-structure size must be nontrivial in comparison with length scales in the experiment. This is a necessary but not a sufficient condition. Indeed, a composite containing aluminum beads in an epoxy matrix was tested for Cosserat effects but it was found to behave according to classical elasticity [14].

The Cosserat characteristic length for a polycarbonate honeycomb was determined [22] from experimental strain and displacement fields. Warp in torsion of a square cross section bar is predicted to be reduced [23] in comparison with classical predictions. Strain distributions were experimentally measured in square cross-section bars of human compact bone [24] and found to follow the Cosserat prediction. Holographic methods disclosed [25] deformation occurred in the corners where it would be classically zero. Holographic methods also revealed reduced warp deformation in square bars of closed cell foam [26], following Cosserat elasticity.

The present research deals with size effects in a designed tetragonal polymer lattice. This lattice was shown, both numerically and experimentally in a companion paper to have a negative Poisson's ratio, tunable via geometric variables [27]. For a lattice of the type studied here, Poisson's ratio is -0.5 for stress applied in the axial direction.

2 Methods

2.1 Materials and experiment

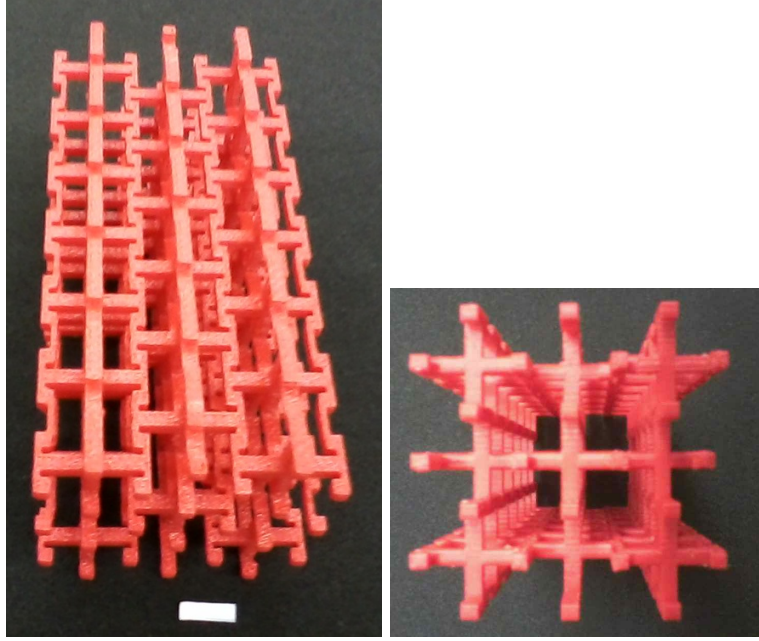


Figure 1: Tetragonal lattice structure (left). Scale bar, 1 cm. End view (right).

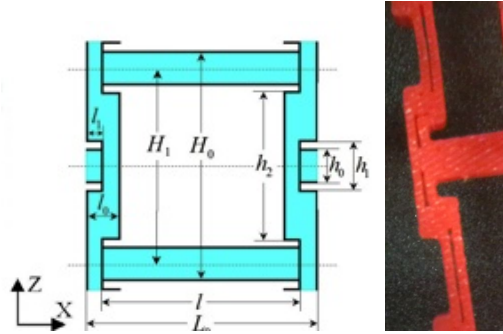


Figure 2: Diagram (left) showing dimensions adapted from [27]. Slot (right) in present specimens.

Lattices (Figure 1) were designed as described in a companion paper [27] and were made using a Stratasys Dimension Elite 3D printer. The parent material was ABS polymer with a claimed Young's modulus of 2.2 GPa and a Poisson's ratio of 0.39. The print resolution is 0.25 mm. The mid-size sample was 100 mm in height and 47.5 mm for the side length. Lattice specimens were cemented to metal end pieces to provide appropriate boundary conditions. Dimensions (Figure 2) of the original lattice were $H_0 = 17.5$ mm, $L = 17.5$ mm, $l = 15.3$ mm, $l_0 = 2.5$ mm, $l_1 = 1.3$ mm, $h_0 = 2.5$ mm, $h_1 = 5$ mm, $h_2 = 10$ mm. Dimensions of the present lattice were essentially identical, within the resolution limit of the printer, $H_0 = 17.7$ mm, $H_1 = 14.9$ mm, $L = 17.5$ mm, $l = 14.9$ mm, $l_0 = 2.5$ mm, $l_1 = 1.3$ mm, $h_0 = 2.7$ mm, $h_1 = 5$ mm, $h_2 = 10$ mm.

Tests were done in compression to evaluate the behavior in the absence of macroscopic gradients of strain and rotation. This was done using a test frame at constant strain rate. Poisson's ratio was also determined using compression testing by measuring the transverse deformation via digital photography and via a micrometer. Torsional and bending rigidity of lattice specimens of different size were determined via broadband viscoelastic spectrometry (BVS). The BVS device generates torque using a dual Helmholtz coil acting upon a magnet attached to the specimen's end piece. The magnet was centered in the coil. Deformation is measured by measuring the position of a reflected laser beam using a digital sensor. The sensor was calibrated using a precision micrometer. Specimens were too large to fit in the coil, therefore an alumina stalk with a magnet on one end was fixed to the lower end plate. The laser mirror was attached to the lower end plate to avoid any error from compliance of the stalk. A mirror was also attached to the upper end plate and further measurements conducted to evaluate the effect of instrument compliance.

Magnet calibration in the BVS was done as in prior studies with this instrument. Torque and angular displacement of a rod of 6061 aluminum alloy of known elastic properties were measured. The torsion calibration constant was 3.81×10^{-4} Nm/A and the bending one was 6.50×10^{-4} Nm/A. The specimen top end plate was attached to a 25 mm diameter steel rod to support the specimen inside the BVS. Viscoelastic deformation was allowed to recover overnight prior to tests to enable stable measurements.

A 1 Hz sinusoidal signal from a SRS Model DS345 function generator was input first to the torsion Helmholtz coil, then to the bending coil. This is well below any resonant frequencies. The same frequency was used for all specimens so viscoelastic effects are decoupled from the size effects to be probed. Torque was inferred from the voltage across a 1Ω resistor in series with the coil. The signals for torque vs. angular displacement were displayed as a Lissajous figure on a digital oscilloscope (Tektronix TDS3014B) using DC coupling. Effective modulus was inferred from torque and angle signals. The maximum strain was less than 2×10^{-5} . This is well within the range of linearity for this material. Linearity was verified from the shape of the load deformation curves.

2.2 Analysis and interpretation

Size effect results were interpreted in the context of Cosserat elasticity. Approximate solutions of the bending and torsion problems are available. The bending rigidity ratio for a rectangular cross section bar of width a depends on both the characteristic length and on Poisson's ratio [28]. If $\beta/\gamma = -\nu$, the rigidity ratio $\Omega = \frac{M}{1/R EI}$ is, with M as moment and R as radius of curvature,

$$\Omega = [1 + 24(\ell_b/a)^2(1 - \nu)]. \quad (12)$$

For other values of Poisson's ratio, the ratio is, (to fourth order in ℓ_b/a),

$$\Omega = \left[1 + 24 \frac{1 + 2\frac{\beta}{\gamma}\nu + \nu^2}{1 + \nu} \left(\frac{\ell_b}{a}\right)^2 - 480 \left(\frac{\beta}{\gamma} + \nu\right)^2 \frac{44 - 38\nu + 3N^2(1 - \nu)(13 - 9\nu)}{N^2(1 + \nu)(22 - 19\nu)} \left(\frac{\ell_b}{a}\right)^4 \right]. \quad (13)$$

Torsion of a square cross section Cosserat elastic bar of width a gives rise to the following relation between torque and angle. When $\kappa \rightarrow \infty$, which corresponds to the coupling number $N = 1$, the total torque M [29] simplifies to

$$M = \frac{4}{21} G \left(\frac{a}{2}\right)^4 \theta \frac{1796 + 126(449 + 2740\bar{\ell}^2 + 3960\bar{\ell}^4)\bar{\ell}^2 + 693(152 + 2280\bar{\ell}^2 + 6615\bar{\ell}^4)\bar{\ell}_b^2}{8(19 + 465\bar{\ell}^2 + 990\bar{\ell}^4) + 1485(6 + 49\bar{\ell}^2)\bar{\ell}_b^2}. \quad (14)$$

in which $\bar{\ell} = 2\ell_t/a$, $\bar{\ell}_b = 2\ell_b/a$ and θ as the angular displacement per length. This solution is superior in the regime of strong coupling or for $\beta/\gamma < 0$, to that of [23], which overestimates the effects for large N .

Because the solid is not isotropic, no attempt was made to further refine the interpretation. No analytical solutions for interpretation are known for anisotropic solids. Elastic constants determined via such a procedure are technical constants. Similarly, classical elastic constants as technical constants for anisotropic materials are obtained from results of standard tensile or compressive tests in principal directions. Size effects do not occur in classical anisotropic elasticity [30]; rigidity depends on thickness as it does in isotropic elasticity. Size effects are therefore a manifestation of nonclassical elasticity and cannot be explained by anisotropy.

In prior studies on round specimens, size effect results were interpreted using exact analytical solutions involving Bessel functions [14] [15].

If either $N \rightarrow 1$ or the specimen is much thicker than the characteristic length, the relations for round specimens are simpler than the exact solutions: $\Omega \approx (1 + 6(\ell_t/r)^2)$ for torsion and $\Omega \approx 1 + 8(\ell_b/r)^2 \frac{(1-(\beta/\gamma)^2)}{(1+\nu)}$ for bending. Size effects in both square and round specimens give rise to higher effective moduli in slender specimens than in thick ones.

For materials with small characteristic length, asymptotic values of G and E are easily determined from sufficiently thick specimens. For materials with large structure size, there is an upper limit to the thickness that can be tested with the present method. Consequently, compression testing was performed to determine the asymptotic value of E in the absence of gradients. The characteristic lengths ℓ_t and ℓ_b were determined by fitting the torsion data to Eq. 14 and the bending data to Eq. 12 using MATLAB.

3 Results and discussion

Specimens 3D printed for size effect studies had a slender pore or slot in some ribs as shown in Figure 2. Compression moduli were measured as 19.4 MPa for the 4x4 specimen, 20.4 MPa for the 2x2 specimen (Figure 1), and 25.7 MPa for the 1x1 specimen, all with the same orientation of ribs. The specimen studied in the companion paper [27] on Poisson's ratio was slightly different in the 3D printed structure; the ribs had no such slot. The relative density was 0.092. The average density of the present specimens was 0.087 g/cm³. Assuming the density of solid ABS polymer as 1.04 g/cm³, the relative density is 0.084. The difference is attributed to variance in the 3D printing process. Results of torsion size effect experiments and interpretation via Eq. 14 are shown in Figure 3.

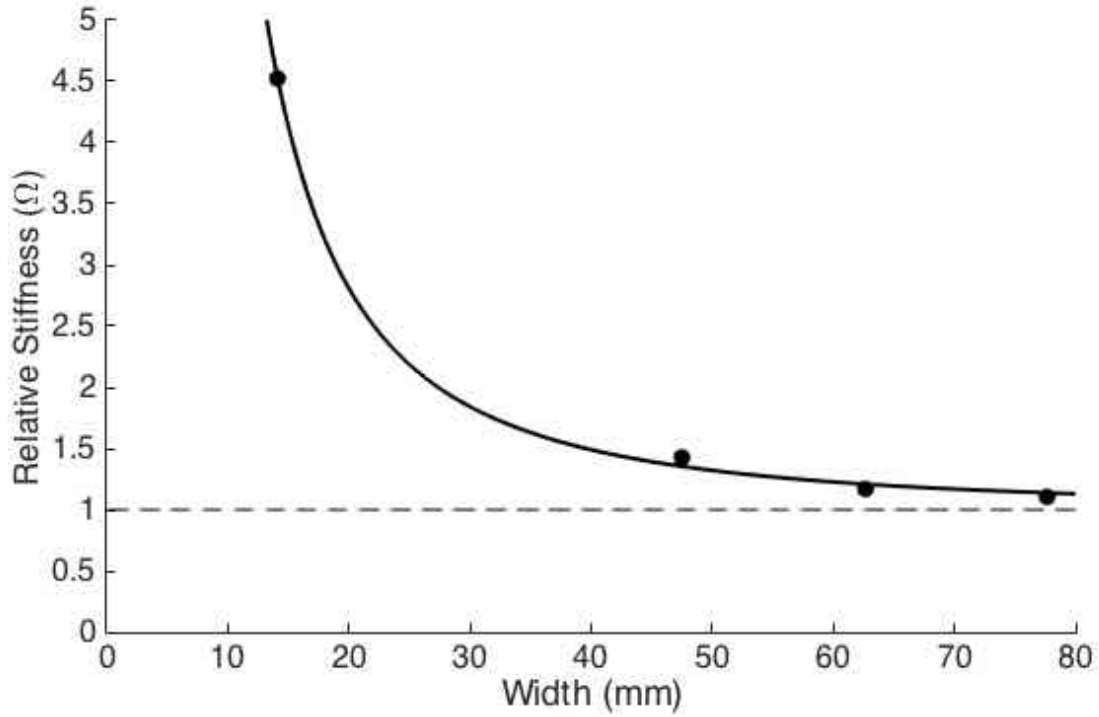


Figure 3: Size effects for lattice specimens in torsion. Points are experimental. Curve is theoretical for $G = 0.67$ MPa, $l_t = 5.6$ mm, $l_b = 10$ mm, $N = 1$. Classical elasticity ($l_t = 0$) predicts constant $\Omega = 1$ independent of diameter which is indicated by the horizontal dashed line.

For specimens in torsion, $G = 0.67$ MPa, $l_t = 5.6$ mm, $l_b = 10$ mm. The goodness of fit was $R^2 = 0.999$. The maximum size effect in torsion was $\Omega = 4.5$. The rigidity expressed in Eq. 14 is strongly dependent on l_t and weakly dependent on l_b . The asymptotic value of G was located via the curve fit. The characteristic length is about a third the cell size.

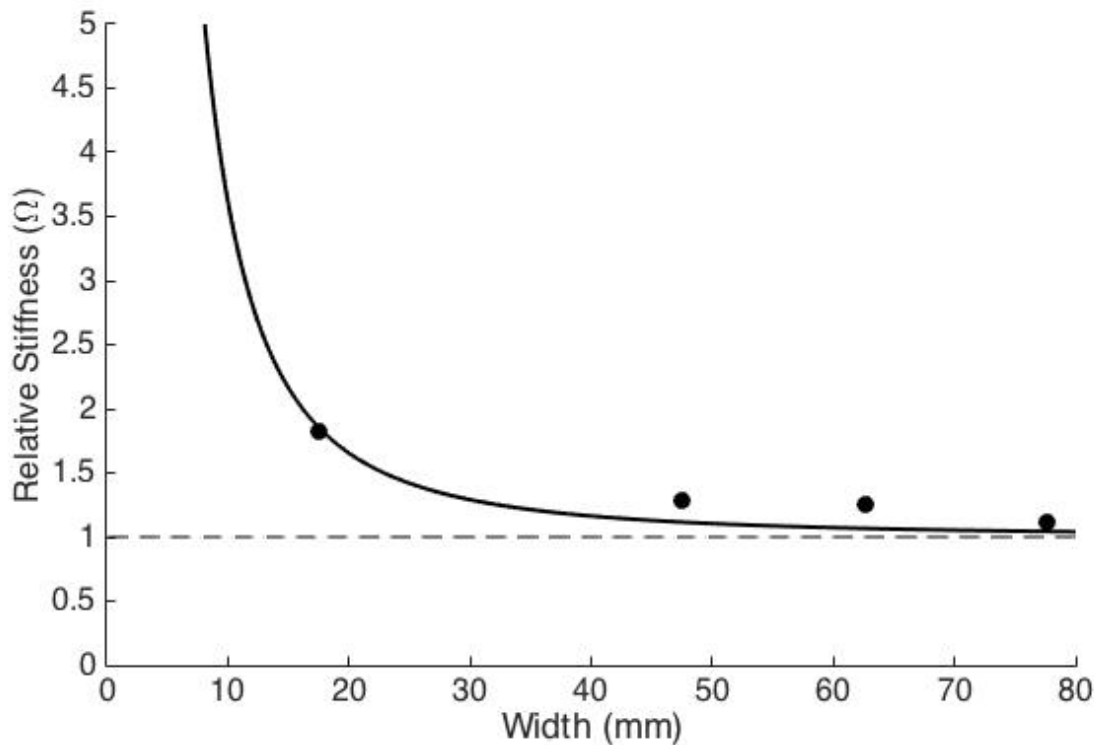


Figure 4: Size effects for lattice specimens in bending. Points are experimental. Curve is theoretical for $\ell_b = 5.4$ mm, $\beta/\gamma + \nu = 0.002$, $N = 0.46$, via Eq. 13. Classical elasticity predicts constant $\Omega = 1$ independent of diameter which is illustrated by the horizontal dashed line.

Results of the bending size effect studies based on fit to Eq. 13 are shown in Figure 4, $\ell_b = 5.4$ mm, $\beta/\gamma + \nu = 0.002$, $N = 0.46$, $\nu = -0.5$. The asymptotic value for $E = 27.6$ MPa was found by as follows. The compression modulus obtained at constant strain rate corresponds to a test at a low frequency. This modulus was converted to a compression modulus at 1 Hz via interrelation among viscoelastic functions using the average loss tangent (0.27) of the largest three specimens. The goodness of fit was $R^2 = 0.75$. Because the composite specimens were anisotropic the characteristic length of bending is independent of the characteristic length of torsion. Anisotropy implies the coupling number N for torsion need not equal the value for bending.

The material has tetragonal structural symmetry. Elastic behavior is therefore anisotropic. Consequently the properties obtained from the experiments are technical constants, not tensorial constants. This is analogous to materials testing in classical elasticity in which it is not always practical to incorporate a full anisotropic interpretation. No analytical solutions are available for tetragonal Cosserat elasticity. Therefore the elastic constants obtained are interpreted as technical constants. Anisotropy is not a confounding variable because size effects do not occur in classical elasticity even in the anisotropic case [30].

Homogenization analyses have been done for several lattices with straight ribs [31] [32] [33]. These lattices are stretch dominated: the overall lattice modulus is governed by axial deformation (stretching or compressing), of the rib elements. Consequently the effects of rib bending and torsion, which govern the Cosserat constants, are much smaller than the effects of rib extension. The Cosserat characteristic lengths of such stretch dominated lattices are much smaller than the cell

size. By contrast, analysis of two dimensional chiral honeycomb lattice revealed bend dominated behavior. The Cosserat characteristic length ℓ is comparable to the cell size [34]. Moreover in such honeycomb, N approaches its upper bound 1. In open cell foams [19] and in negative Poisson's ratio foams [20] derived from them, ℓ is greater than the cell size. Specifically, ℓ_t is a factor 1.8 to 4 greater than the cell size, and ℓ_b is a factor 4.9 to 7.5 greater than the cell size, depending on the kind of foam. Such foams are highly bend dominated. Cosserat effects are therefore considerably stronger in bend dominated lattices and materials studied thus far than in stretch dominated ones. The present lattice is considered bend dominated based upon dependence of the modulus on relative density of the lattice [27]. However the ribs are aligned so that the axial modulus is enhanced. The Cosserat characteristic length of cellular solids depends on the ratio of torsion and bend rigidity of *ribs* to their axial rigidity. Therefore it is to be expected that the Cosserat effects are not as pronounced as in foams. The ratio of characteristic length to cell size is larger than in fully stretch dominated lattices but smaller than in bend dominated honeycombs or foams.

Cosserat elasticity facilitates understanding of size effects due to distributed torques propagated through the structure of a heterogeneous material. Size effects may rise from a variety of causes. In foams, a layer of surface damage can give rise to a softening effect in which slender specimens appear more compliant than large ones [35]; this effect is opposite that in Cosserat solids. Edge effects in 2D negative Poisson's ratio structures of rotating squares have been predicted [36]. The apparent rigidity for axial tension depends on size as a result of the boundary conditions being different from conditions in the bulk. These effects differ from effects in Cosserat solids in that (i) they are not driven by gradients, and (ii) unlike Cosserat effects they do not obey Saint Venant's principle. Cosserat size effects are driven by gradients that occur in torsion and bending; the bar can be arbitrarily long; there are no size effects in tension.

Cosserat elasticity has also been used in analysis of granular materials [37]; a Cosserat fluid model successfully describes collisional granular flows on a slope [38]. 2D ensembles of hard disks in an enclosure have been studied from a thermodynamic perspective [39]; elastic aspects were considered in a classical context [40]. In such systems, size effects might occur due to exclusion of discs by the boundary in contrast to Cosserat type effects due to moments. If rotational energy is considered, there will be a conceptual link with the Cosserat approach.

Size effects are not the only result of nonzero structure size interpreted via Cosserat elasticity. Stress concentrations associated with holes are reduced in comparison with classical predictions [16]; the effect is more pronounced for small holes. Similarly stress concentration around a notch is reduced in comparison with predictions of classical elasticity. The result is improved toughness in the presence of such defects.

In summary, size effects are observed in torsion and in bending of tetragonal auxetic lattices. The lattices are therefore not classically elastic. The size effects are interpreted via Cosserat elasticity. Continuum theories with more freedom, e.g. micromorphic / Mindlin microstructure [41] elasticity or microstretch elasticity [42] are not excluded; they are not necessary for the present observations. For example, the Mindlin elasticity theory, in which *points* translate, rotate, and deform, allows 18 elastic constants for an isotropic solid, and microstretch elasticity allows 9 constants for an isotropic solid.

4 Conclusions

Size effects occur in the torsion and bending of lattice structures. These effects are not consistent with classical elasticity. They are interpreted with Cosserat elasticity. The characteristic lengths are about a third of the cell size. The Cosserat torsional characteristic length is $\ell_t = 5.6$ mm. The

bending characteristic length is $\ell_b = 5.4$ mm. The size effect in torsion is a factor 4.5 in rigidity.

5 Acknowledgements

We gratefully acknowledge partial support of this research by the National Science Foundation via Grant CMMI-1361832. We also acknowledge partial support by The National Natural Science Foundation of China (11304033) and the Fundamental Research Funds for the Central Universities (N150504006). D. Li would also like to thank the financial support from the China Scholars Council (File No. 201506085013).

References

- [1] L. J. Gibson, M. F. Ashby, G. S. Schajer, and C. I. Robertson, The mechanics of two dimensional cellular solids, Proc. Royal Society London, **A382**, 25-42 (1982).
- [2] R. S. Lakes, Foam structures with a negative Poisson's ratio, *Science*, **235** 1038-1040 (1987).
- [3] S. Burns, Negative Poisson's ratio materials, letter, *Science*, **238**, 551 (1987).
- [4] R. S. Lakes, Negative Poisson's ratio materials, response *Science*, **238** 551 (1987).
- [5] S. Hirotsu, Elastic anomaly near the critical point of volume phase transition in polymer gels. *Macromolecules* **23**, 903-905 (1990)
- [6] R. E. McKnight, A. Moxon, A. Buckley, P. A. Taylor, T. W. Darling, and M. A. Carpenter, Grain size dependence of elastic anomalies accompanying the alpha-beta phase transition in polycrystalline quartz. *J. Phys. Cond. Mat.* **20**, 075229 (2008)
- [7] K.W. Wojciechowski, Constant thermodynamic tension Monte Carlo studies of elastic properties of a two-dimensional system of hard cyclic hexamers, *Molecular Physics* **61**, 1247-1258, (1987).
- [8] K. V. Tretyakov and K. W. Wojciechowski, Orientational transition between isotropic crystalline phases in planar systems of hard cyclic pentamers and heptamers, *Journal of Physics: Condensed Matter* **14**, 1261 (2002)
- [9] K. V. Tretyakov and K. W. Wojciechowski, Monte Carlo simulation of two-dimensional hard body systems with extreme values of the Poisson's ratio, *Physica Status Solidi B* **242**, 730-741 (2005).
- [10] S. P. Timoshenko, *History of Strength of Materials*, Dover, NY, (1983).
- [11] E. Cosserat, and F. Cosserat, *Theorie des Corps Deformables*, Hermann et Fils, Paris (1909).
- [12] A.C. Eringen, Theory of micropolar elasticity. In Fracture Vol. **1**, 621-729 (edited by H. Liebowitz), Academic Press, New York (1968).
- [13] L. J. Gibson, and M. F. Ashby, *Cellular Solids*, 2nd Ed., Cambridge, (1997).
- [14] R. D. Gauthier and W. E. Jahsmann, A quest for micropolar elastic constants. *J. Applied Mechanics*, **42**, 369-374 (1975).

- [15] G. V. Krishna Reddy and N. K. Venkatasubramanian, On the flexural rigidity of a micropolar elastic circular cylinder, *J. Applied Mechanics* **45**, 429-431 (1978).
- [16] R. D. Mindlin, Effect of couple stresses on stress concentrations, *Experimental Mechanics*, **3**, 1-7, (1963).
- [17] R. S. Lakes, Experimental microelasticity of two porous solids, *Int. J. Solids and Structures*, **22**, 55-63 (1986).
- [18] W. B. Anderson and R. S. Lakes, Size effects due to Cosserat elasticity and surface damage in closed-cell polymethacrylimide foam, *J. Materials Science*, **29**, 6413-6419 (1994).
- [19] Z. Rueger and R. S. Lakes, Experimental Cosserat elasticity in open cell polymer foam, *Philosophical Magazine*, **96**, 93-111 (2016).
- [20] Z. Rueger and R. S. Lakes, Cosserat elasticity of negative Poisson's ratio foam: experiment, *Smart Materials and Structures*, **25**, 054004, 8pp, (2016).
- [21] R. S. Lakes, On the torsional properties of single osteons, *J. Biomechanics*, **28**, 1409-1410 (1995).
- [22] R. Mora and A. M. Waas, Measurement of the Cosserat constant of circular cell polycarbonate honeycomb, *Philosophical Magazine A*, **80**, 1699-1713 (2000).
- [23] H. C. Park and R. S. Lakes, Torsion of a micropolar elastic prism of square cross section. *Int. J. Solids, Structures*, **23**, 485-503 (1987).
- [24] H. C. Park and R. S. Lakes, Cosserat micromechanics of human bone: strain redistribution by a hydration-sensitive constituent, *J. Biomechanics*, **19**, 385-397 (1986).
- [25] R. S. Lakes, D. Gorman, and W. Bonfield, Holographic screening method for microelastic solids, *J. Materials Science*, **20**, 2882-2888 (1985).
- [26] W. B. Anderson, R. S. Lakes, and M. C. Smith, Holographic evaluation of warp in the torsion of a bar of cellular solid, *Cellular Polymers*, **14**, 1-13 (1995).
- [27] D. Li, J. Ma, L. Dong and R. S. Lakes, Three-dimensional stiff cellular structures with negative Poisson's ratio, *Physica Status Solidi B* accepted June (2017).
- [28] R. S. Lakes and W. J. Drugan, Bending of a Cosserat elastic bar of square cross section - theory and experiment, *J. Applied Mechanics*, **82**(9), 091002 (2015).
- [29] W. J. Drugan, Torsion of a Cosserat elastic bar of square cross section, in preparation (2017).
- [30] S. G. Lekhnitskii, *Theory of elasticity of an anisotropic body*, Mir, Moscow, (1981).
- [31] A. Askar and A. S Cakmak, A structural model of a micropolar continuum, *Int. J. Engng. Sci.* **6**, 583-589, (1968).
- [32] T. Tauchert, A lattice theory for representation of thermoelastic composite materials, *Recent Advances in Engineering Science*, **5**, 325-345 (1970).
- [33] G. Adomeit, Determination of elastic constants of a structured material, *Mechanics of Generalized Continua*, (Edited by Kröner, E.), IUTAM Symposium, Freudenstadt, Stuttgart. Springer, Berlin (1967).

- [34] A. Spadoni and M. Ruzzene, Elasto-static micropolar behavior of a chiral auxetic lattice, *J. Mechs Physics of Solids*, **60**, 156-171 (2012).
- [35] R. Brezny and D. J. Green, Characterization of edge effects in cellular materials *J Materials Sci*, **25** 4571-4578 (1990).
- [36] R. Gatt, R. Caruana-Gauci, D. Attard, A. R. Casha, W. Wolak, K. Dudek, L. Mizzi, and J. N. Grima, On the properties of real finite-sized planar and tubular stent-like auxetic structures, *Phys. Status Solidi B* **251**, No. 2, 321-327 (2014).
- [37] L La Ragione and J T Jenkins, The influence of particle fluctuations on the average rotation in an idealized granular material, *Journal of the Mechanics and Physics of Solids* **57**, (9) 1449-1458 (2009).
- [38] N Mitarai, H Hayakawa, and H Nakanishi, Collisional Granular Flow as a Micropolar Fluid, *Phys. Rev. Lett.* **88**, 174301 (2002).
- [39] K. W. Wojciechowski, P. Pierarlski, and J. Malecki, A hard-disk system in a narrow box. I. Thermodynamic properties, *J. Chem. Phys.*, **76**, 6170-6175 (1982).
- [40] K. W. Wojciechowski K. V. Tretiakov A. C. Branka and M. Kowalik Elastic properties of two-dimensional hard disks in the close-packing limit *J. Chem. Phys.*, **119**, 939-946 (2003).
- [41] R. D. Mindlin, Micro-structure in linear elasticity, *Arch. Rational Mech. Analy*, **16**, 51-78, (1964).
- [42] A. C. Eringen, Theory of thermo-microstretch elastic solids, *Int. J. Engng. Sci.*, **28** (12) 1291-1301, (1990).